A Rapid Method for Matching Pair Determination from Disordered and Massive Asteroid Images

ZHANG Jiujiang[1, 2, 3]，GENG Xun[1, 2, 3]，YU Junming[4]，LIU Jie[4]，
LIU Pengying[1, 2, 3]，PENG Zhen[1, 2, 3]，MA Xin[3, 5]

（1. College of Geographical Sciences, Faculty of Geographical Science and Engineering, Henan University，Zhengzhou 450046，China；
2. State Key Laboratory of Geo-Information Engineering，Xi'an 710054，China；
3. Henan Industrial Technology Academy of Spatio-Temporal Big Data，Zhengzhou 450046，China；
4. China Electronic Technology Group Corporation 27th Research Institute，Zhengzhou 450047，China；
5. School of Computer and Information Engineering，Henan University，Kaifeng 475004，China）

Abstract： This paper proposed an efficient method of image overlapping relationship analysis based on spatial index of KD tree fast search for disordered and large-scale asteroid images. In this study, the image data from asteroid exploration missions such as Bennu, Vesta, and Ryugu were used for experiments, and the proposed image matching pairs determination algorithm was comprehensively compared with the corresponding modules of USGS ISIS in order to evaluate its performance in terms of efficiency and accuracy. The results show that when processing more than a thousand images, the proposed method greatly improves the efficiency of acquiring image matching pairs while ensuring the correctness of image overlapping relationships and accuracy of bundle adjustment. At the same time, according to the obtained image matching pairs, images that meet the requirements of Stereo Photoclinometry can be quickly selected, effectively improving the quality of 3D reconstruction models of asteroid images.

Keywords： asteroid exploration；photogrammetry；image matching；KD tree；image matching pairs

Highlights：

- An efficient image matching pair determination method based on KD tree and radius range search was proposed, which greatly improved the efficiency of computing the overlapping relationship for massive asteroid remote sensing images.
- A method based on light ray intersection of sampling points was proposed for acquiring the real image center for abnormal asteroid images (i.e., images containing invalid pixels), especially for low-resolution images during the approaching stage.
- The image matching pairs determined by the proposed method can effectively facilitate the selection of the best images for SPC reconstruction.

中图分类号：P185.7　　文献标识码：A　　文章编号：2096-9287(2025)05-0542-15

DOI:10.3724/j.issn.2096-9287.2025.20250007

Reference format: ZHANG J J，GENG X，YU J M，et al. A rapid method for matching pair determination from disordered and massive asteroid images[J]. Journal of Deep Space Exploration, 2025, 12 (5) : 542-556.

引用格式：张九江，耿迅，于君明，等. 一种海量无序小行星遥感影像匹配对快速确定方法[J]. 深空探测学报（中英文），2025，12（5）：542-556.

Introduction

In recent years, asteroids have become the main targets of deep space exploration missions[1-3]. High-precision mapping products of an asteroid's surface are important basic data for asteroid exploration mission implementation and scientific research[4-6]. Multiple asteroid exploration missions, such as OSIRIS-REx for Bennu in the United States[7], Hayabusa-2 for Ryugu in Japan[3] and DAWN for vesta in the United States[8], have achieved fruitful mapping products[9-12]. These missions

收稿日期：2025-01-23　修回日期：2025-05-26

基金项目：Space Optoelectronic Measurement and Perception Lab （LabSOMP-2023-07）；the National Natural Science Foundation of China （42241147）；the State Key Laboratory of Geo-Information Engineering （SKLGIE2021-Z-3-1）；and the Open Program of Collaborative innovation Center of Geo-information（2023C002）

have acquired a large number of high-resolution remote sensing images, which provide rich data resources for scientific research and generating mapping products[13].

In the process of generating planetary mapping products, photogrammetry is the main technical means[14-15]. However, with the increase in the number of exploration missions, the amount of image data grows exponentially. Actual planetary photogrammetry projects may consist of tens of thousands or even millions of unordered images, significantly increasing the processing difficulty[16-19]. Due to the complex topography and irregular shape of the asteroid surface and the complexity of the planetary photogrammetric processing process itself, the efficient processing of massive asteroid remote sensing images has become a technical bottleneck in the current field of asteroid remote sensing mapping. Therefore, the method by which to efficiently and accurately obtain overlapping image match pairs of large-scale unordered images has become one of the key issues in asteroid remote sensing mapping. If only simple brute-force matching is used to obtain image match pairs, the efficiency will be very low.

Regarding the determination of overlapping relationships for unordered images, a large amount of research has been carried out in the field of Earth observation. For example, in the field of Unmanned Aerial Vehicle (UAV) photogrammetry, Liang et al.[20] used existing geospatial data and prior knowledge to generate accurate match pairs, which has high efficiency and accuracy for large-scale UAV photogrammetry. Jiang et al.[21] proposed a method to provide efficient matching pair selection for oblique UAV images. This method includes designing image and feature selection strategies to reduce redundancy, implementing an adaptive threshold selection method to determine the number of candidates match pairs, and proposing the adaptive vocabulary tree expansion algorithm for selecting and simplifying match pairs. Subsequently, in 2023, Jiang et al.[22]. optimized this matching pair selection method This optimization aggregates local features of images and converts them into high-dimensional global descriptors, thereby effectively reducing the number of features and the burden of nearest neighbor search. At the same time, global descriptors are indexed through a specific graph structure, and an adaptive threshold selection strategy is used to efficiently retrieve match pairs. Rupnik et al.[23] provided an efficient and accurate solution for the automatic orientation of large-scale oblique images based on a connection graph method. By constructing and optimizing the connection graph, the overlapping relationships between images can be quickly determined. In the field of computer vision, Chen et al.[24-25] developed a modified Siamese network Overlap Net, which can be used to predict the overlap of images at a certain distance generated by 3D lidar scanning. However, these methods are mainly for airborne remote sensing images in the field of Earth observation and rely on POS information, which cannot be directly used for the processing of planetary remote sensing images, and are less applicable to irregular asteroid images.

In addition, some open-source photogrammetric software in planetary mapping community provides programs to determine the image pairs. For example, the Integrated System for Imagers and Spectrometers (ISIS) software developed by the United States Geological Survey (USGS) provides modules such as *footprint* and *findimageoverlaps* for calculating image overlapping relationships, which is a prerequisite for subsequently establishing a control network and performing bundle adjustment. This algorithm first uses the initial camera position and attitude information to calculate the ground point coordinates of the image, and then uses the ground point coordinates to form a polygon in two-dimensional space. The overlapping relationships between images is determined by judging the overlap of polygons. Although this method combines the initial pose information of the image, the computational complexity is exponentially related to the number N of ground point coordinates on the image, namely $O(N^2)$. In our experiments, we found that due to the exponential algorithm complexity, it usually takes several hours or even days to process a large amount of disordered asteroid remote sensing images (e.g., thousands of images), which is extremely inefficient[26]. Although the Ames Stereo Pipeline (ASP) developed by the National Aeronautics and Space Administration (NASA) has accelerated the parallel computation of the planetary remote sensing image matching process, it lacks a module similar to the USGS ISIS for calculating image overlapping relationships. Therefore, it can only construct the control networks by brute-force matching[27-28].

In addition, in the field of planetary photogrammetry, the Stereo PhotoClinometry (SPC) method, as an approach of reconstructing more detailed three-dimensional terrains, has opened a new avenue for obtaining higher-resolution terrain models[29]. During the process of planetary exploration, factors such as the complexity of spacecraft observation environments, illumination conditions, and the irregular shape of the asteroids, result in that the acquired image data exhibits characteristics of multiple overlaps and disorder. Moreover, SPC reconstruction has relatively high requirements for the observation and illumination conditions of the images[30], and it also has a strong dependence on the correct overlapping relationships between the images. The method by which to efficiently select the images suitable for SPC reconstruction from the vast and image data has become a crucial issue. In this context, a fast and efficient method for determining image overlapping relationships becomes particularly important.

In this context, a fast and efficient method for determining image overlapping relationships becomes particularly important. This paper proposes a fast and accurate method for determining image match pairs based on the KD tree for irregular asteroid images. The core idea of the method is based on the high efficiency of spatial search of the KD tree[31] to determine image overlapping relationships between the image to be searched and its surrounding images. The proposed method uses the three-dimensional coordinates of the center point of the image to construct the KD tree and then performs range search according to the specified search radius. To further enhance the applicability of the proposed method, we also design an algorithm to determine the real valid image center for asteroid remote sensing images containing invalid pixels. The proposed method can not only effectively reduce the invalid match pairs and greatly decrease the image matching time during experimental processing, but also optimally select the images that meet SPC requirements based on the acquired image match pairs. The proposed method in this paper is a very efficient and robust means for calculating the overlapping relationships of massive unordered asteroid remote sensing images, simplifying later photogrammetric processing.

1 Materials and Methods

1.1 Overall Algorithm Process

To solve the problem of calculating the match pairs of massive asteroid remote sensing images, this paper proposes an efficient method based on the KD tree quick search. This process combines SPC and image match pairs. The blue parts of the figure show the corresponding modules of ISIS and the green boxes show the methods for determining the image centroid in different exploration stages. The detailed process is shown in Fig.1.

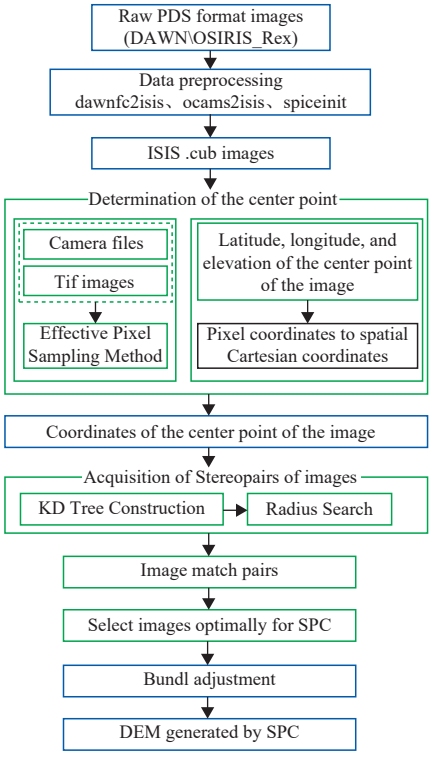

Fig. 1 Overall flowchart

1.2 Basic Principle of Determining Image Match Pairs

The proposed method in this paper mainly determines the match pairs of massive asteroid remote sensing images by combining the KD tree structure and R radius range search. Although the performance of the KD tree will decline in high-dimensional space, it performs best when processing low-dimensional space[32-33]. The proposed algorithm constructs a three-dimensional KD tree based on the space rectangular coordinates of the center point of the image, which is exactly in a low-dimensional space. After constructing the KD tree, R radius range search is conducted to determine the overlapping images through

computing the Euclidean distance of different center points of images[34-35]. The principle of R range search is to use the distance between the centers of two images as the farthest overlapping pixel of the search radius; that is, the distance of the central point in the three-dimensional space is estimated by utilizing the geometric information of the two images. Then, the search radius is determined in combination with the image resolution. The calculation formula is as follows:

$$R_{\text{threshold}} = W \times R \times d \tag{1}$$

where W is the width or height of the image size, R is the image resolution, d is the minimum overlap, and $R_{\text{threshold}}$ is the radius search threshold. Fig.2 shows the detailed process for its calculation.

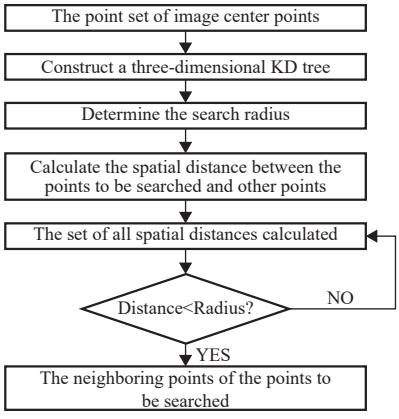

Fig. 2　Flowchart of R range search process based on KD tree structure

When constructing the KD tree and R radius searches, the input data are the three-dimensional coordinates of the center points of asteroid images. Next, we discuss in detail the method for determining the center points of images.

1.3　Determination of the Actual Center Point of the Images

Data preprocessing is first required to determine the center point coordinates of the image. The method adopted in this paper is as follows: First, raw asteroid images in Planetary Data System (PDS) formats are converted into ISIS-cube format (.cub) based on the corresponding software tools provided in USGS ISIS. Then, the geometric coordinates (i.e., latitude, longitude coordinates and elevation) of the center point of the image are extracted from the ISIS .cub image and converted into space rectangular coordinates. However, since the asteroid image data obtained from different exploration stages have large differences in resolution and image quality, it is still uncertain whether the actual center point of the image is located at the center of the image. Therefore, data preprocessing needs to be carried out on image data in different exploration stages.

1.3.1　Normal asteroid remote sensing images

For these image data, such as Bennu data obtained in the Detailed Survey (DS) stage[9,36] and Vesta data obtained in the High-Altitude-Mapping Orbit (HAMO) stage (as shown in Fig. 3(b))[8], we first extract the latitude and longitude coordinates and elevation of the image center point and directly convert them into space rectangular coordinates. The specific process is shown in Fig. 4.

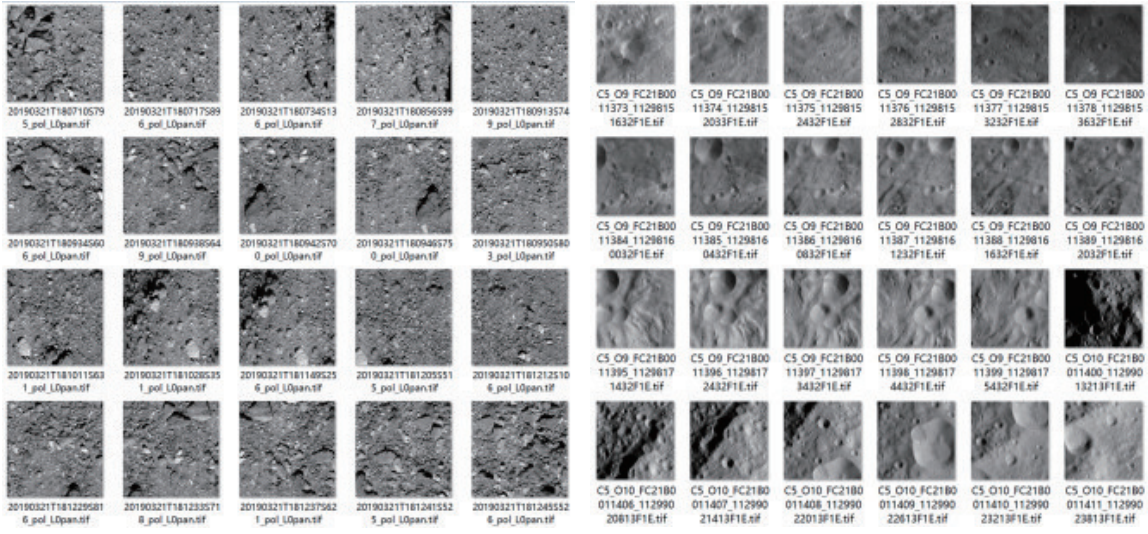

（a）Raw images of Bennu　　（b）Vesta

Fig. 3　Display diagram of normal asteroid remote sensing images

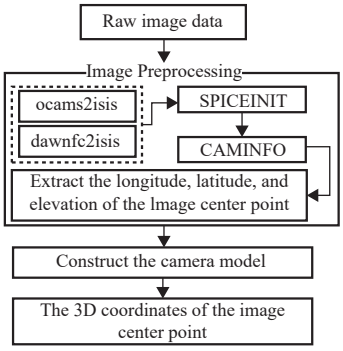

Fig. 4 Flowchart for determining center point of image

1.3.2 Abnormal asteroid remote sensing images containing invalid pixels

For asteroid remote sensing images containing invalid pixels, such as Bennu image data obtained in the Preliminary Survey (PS) stage[9,36] and Ryugu image data obtained in the asteroid characterization phase[10], the center point of the valid pixels is not located at the center of the image (as shown in Fig. 5). When directly using the image center point for determining the space rectangular coordinates, there may be no intersection with the celestial body surface. Thus, it is necessary to recalculate the center point of the valid pixels. This study designs a method for calculating the actual center point of valid pixels based on the ray intersection of sampling points. The core idea of the proposed method is to preset an effective gray threshold for the asteroid remote sensing images. This threshold is determined according to the grayscale histogram of the observed image. Then, the entire image is sampled every 10 pixels in both row and column directions. Each sampling point has its own gray value. We compare the gray value of the sampling point with the specified gray threshold. If the gray value of the sample point is greater than the gray threshold, the sampling point is considered an effective sampling point; otherwise, it is considered an invalid sampling point. Finally, we calculate the average pixel coordinates of all effective sampling points, and take them as the virtual center point of the asteroid image. Then, this virtual center point is used to determine the pixel coordinates of the center point of the image (see Fig. 5). Next, combining the information of the exterior orientation parameters and the constructed camera model, we calculate a spatial three-dimensional direction vector and a three-dimensional point on the image. Using the parametric equation (i.e., point-direction form), a three-dimensional spatial straight line passing through the image center is determined. Finally, we calculate the intersection point of this straight line with a low-resolution 3D model or Digital Elevation Model (DEM) of the target celestial body. When a light ray intersects with an asteroid, there are generally two intersection points, one on the same side of the camera and the other one on the other side of the camera. We choose the intersection point closer to the camera as the final center point of the image. A schematic diagram of the ray intersection of sampling points is shown in Fig. 6, and its specific process is shown in Fig. 7.

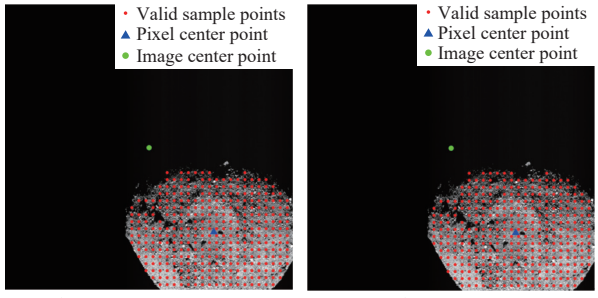

（a）Sampling maps of Bennu （b）Ryugu images

Note: The green circle is the center of the image, and the blue triangle is the valid pixel center of the image.

Fig. 5 Effective pixel sampling process diagram

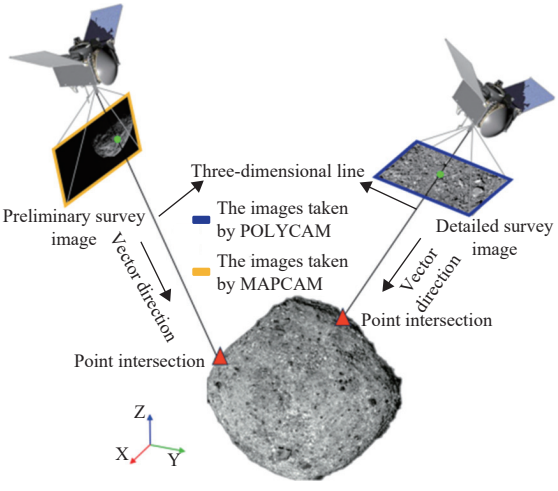

Fig. 6 Schematic diagram of ray intersection of sampling point method

1.4 Optimal Image Selection for SPC Reconstruction

SPC is a method that uses images with different illumination conditions, observation geometries, and pixel scales to generate elaborate three-dimensional terrain which is consistent with the resolution of the original image. It combines stereophotogrammetry (SPG) and

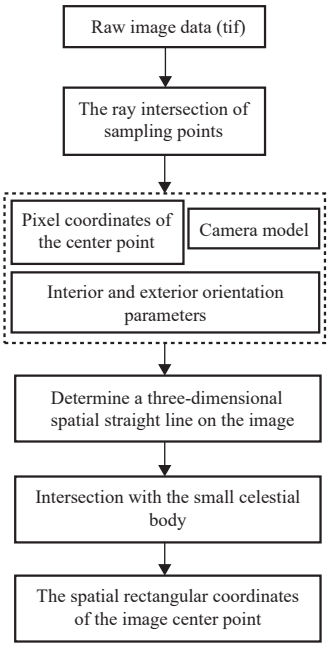

Fig. 7　Flowchart of ray intersection of sampling point method

photoclinometry. The generated products have the accuracy of SPG and the resolution of photoclinometry without being subject to the common limitations of both[36].

Combined with the literature and practical experience[37-40], the ideal illumination and observation conditions for SPC reconstruction are shown in Table. 1. Indeed, the returned asteroid remote sensing images may cover situations taken on different dates, different orbits, and at different times, resulting in problems such as irregular overlap, disorder, and excessive redundancy of the images. In order to ensure the best three-dimensional reconstruction quality, optimal image selection is essential to meet the requirements of SPC reconstruction.

Table 1　Optimal illumination and observation conditions for SPC reconstruction

Image	Technical indicators	Parameter Range
Images focusing on terrain	Incidence angle	30°–50°
	Spacecraft azimuth angle	Shooting in four directions, east, south, west and north, relative to the target area
Images focusing on albedo	Incidence angle	Close to 0°
	Solar azimuth angle	0°–20°

2　Experiment and Analysis

2.1　Test Data

For normal images, we select the image data of Bennu obtained in the detailed survey stage and the image data of Vesta obtained in the HAMO stage. For images containing invalid pixels, we select the image data of Bennu obtained in the preliminary survey stage and the image data of Ryugu obtained in the asteroid characterization phase for processing. These four sets of data are used to evaluate the performance of the proposed algorithm for calculating image match pairs.

In addition, we also use the ISIS software to calculate match pairs for the same data, and conduct a comparative analysis of the time efficiency as well as accuracy. Subsequently, we use the obtained overlapping relationships to extract tie points and construct the control network. Then, we use the ISIS jigsaw module to perform bundle adjustment. In this study, all experiments were executed on a laptop computer configured with 32 GB of RAM, Intel Core (TM) i7-13650HX 2.60 GHz CPU and Ubuntu 22.04 operating system, with ISIS using version 8.0.0. The related software was developed based on C++language, using Point Cloud Library (PCL) for KD tree search. Specific information about the experimental data is shown in Table. 2.

Table 2　Basic information of test data

Data	Cameras	Asteroid	Number of images	Date	Mean GSD/m	Image size (samples × lines)
Test 1	POLYCAM	Bennu	5 453	2019.03.21—04.12	0.05	1 024 × 1 024
Test 2	FC	Vesta	2 553	2011.09.29—10.31	65.00	1 024 × 1 024
Test 3	MAPCAM	Bennu	942	2018.12.03—12.17	1.00	1 024 × 1 024
Test 4	ONC	Ryugu	391	2018.07.10、2018.07.12、2018.08.01	1.50	1 024 × 1 024

Note: GSD refers to ground sample distance. Since the resolutions of the images are not strictly uniform, this study calculates their average values. FC refers to Framing Camera. ONC refers to Optical Navigation Camera.

2.2　Complexity of the Algorithm

In the previous discussion, we introduced the basic principle of determining the match pairs based on the KD tree structure and the valid image center point. Next, we analyze the complexity of the algorithm.

KD tree search can efficiently organize and query multi-dimensional spatial data by using spatial division and partitioning. The proposed algorithm's complexity contains construction complexity and query complexity. When constructing a KD tree, the insertion operation of each node requires O (log N) comparisons in a balanced

case. Therefore, its average time complexity is O (log N) (N represents the number of images). When querying a KD tree, the query process is similar to the search process of a binary tree. Therefore, the average time complexity of nearest neighbor search using a KD tree is O (log N)[41]. In contrast, the Findimageoverlaps software tool provided in USGS ISIS adopts the brute-forcing search method. Indeed, it determines the overlapping relationships of images by analyzing whether polygons composed of footprint coordinates intersect. When determining a potential image matching pair, it is necessary to use all footprint coordinates of an image to form a footprint polygon. Therefore, the time complexity of the software tool provided in USGS ISIS is $O(N \times M)^2$ (N represents the number of images and M represents the number of footprints on the image). The details are shown in Fig. 8 (Fig. 8(a) represents the images and Fig. 8(b) represents the number of foot-points of these images).

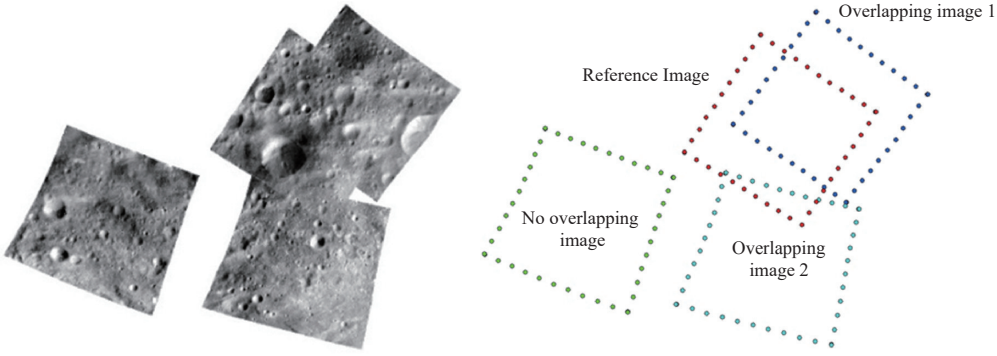

（a）DOM images of Vesta

（b）Footprint coordinates of these images (dots represent the foot points)

Fig. 8 Diagram for determining image matching pairs using USGS ISIS's software tool *findimageoverlaps*

For an asteroid remote sensing image, the number of footprints it contains may be several hundred or even thousands, which depends on the parameter settings when processed by USGS ISIS. Moreover, the images at high latitudes are more stretched, resulting in a larger number of footprints, which leads to longer computation time when calculating the overlapping relationships (as shown in Fig. 9(c)). However, the obtained foot points are the footprints on the projected Digital Orthophoto Map (DOM) image. Therefore, existing methods for calculating the image match pairs still have shortcomings in high-latitude regions. When the number of images N increases, the complexity of the existing methods (e.g., USGS ISIS) rapidly increases, resulting in low efficiency. In contrast, the proposed algorithm only needs to calculate the spatial distance to determine the image overlapping relationships, and it is not affected by different latitudes. Moreover, the time complexity of the proposed algorithm is much lower than the corresponding modules of ISIS software. It is obviously more efficient in processing large-scale data and can significantly improve the speed of determining image match pairs.

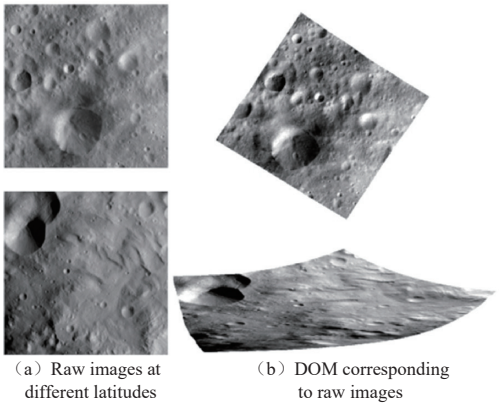

（a）Raw images at different latitudes

（b）DOM corresponding to raw images

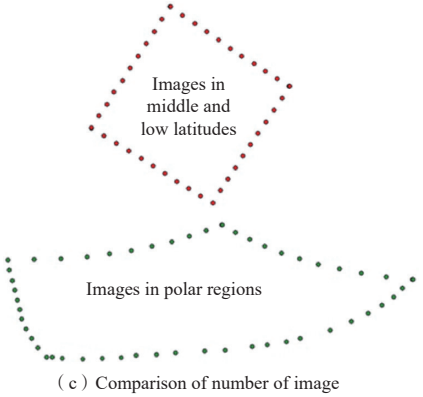

（c）Comparison of number of image footprints at different latitudes

Fig. 9 Images of Vesta at different latitudes

2.3 Experimental results and analysis of determining image match pairs

2.3.1 Experimental results and analysis of determining image match pairs

First, after determining the space rectangular coordinates of the image center point, we used the algorithm described in Section 2.1.1 to obtain the image match pairs of data from Tests 1 and 2. Table. 3 shows the statistical results of the time taken by different methods to calculate image match pairs.

Table 3　Test data for detailed survey images

	Bennu（2019）				Vesta
Number of images	32	255	1365	5453	2553
Time spent on KD tree/s	<1	1	2	3.84	2～3
Time spent on ISIS/s	8	40	300	—	—

Note: "—" indicates that the experiment could hardly be completed.

As can be clearly seen from the table, as the number of images increases, the time taken by the ISIS method increases even exponentially. This shows that the proposed algorithm is clearly superior to the ISIS method when processing a large amount of image data. Due to the images in the polar or high latitude regions have a large stretching problem, resulting in a single image that may span the entire longitude range. Thus, the *findimageoverlaps* module will produce incorrect match pairs, significantly increasing the computation time. Therefore, the existing algorithm adopted in USGS ISIS is not suitable for asteroid images in polar or high-latitude regions. In contrast, the proposed algorithm uses the space rectangular coordinates of the valid center point and is not affected by latitudes. Therefore, the proposed algorithm has better applicability for processing a large number of unordered remote sensing images in practical applications.

To check the correctness of the obtained image match pairs, we open the corresponding images in ISIS's *qmos* program. Fig. 10 and Fig. 11 show the comparison diagrams of the match pairs obtained by the proposed method and the ISIS method. The red image in the figures represents the target image, and the images of other colors represent the overlapping images.

As can be seen, the image match pairs obtained by the proposed algorithm are basically the same as the results obtained by USGS ISIS.

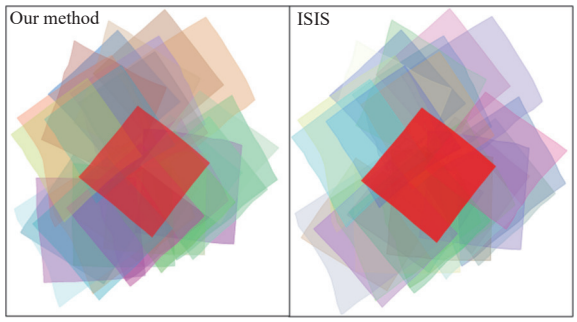

Fig. 10　Comparison of determined image matching pairs for Vesta images in HAMO phase

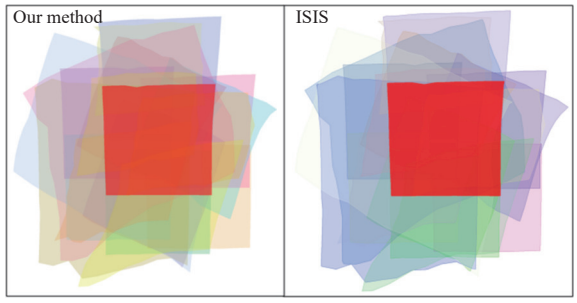

Fig. 11　Comparison of determined image matching pairs for Bennu images in detail survey phase

2.3.2 Abnormal Asteroid Remote Sensing Images Containing Invalid Pixels

The images from Tests 3 and 4 are low-resolution remote sensing images acquired at the approach state of the exploration. Since these low-resolution images contain invalid pixels, ISIS cannot be used to complete the calculation of footprint coordinates. Consequently, ISIS failed to determine the image overlapping relationship. In contrast, the proposed algorithm can calculate the image overlapping relationship for these images based on the space rectangular coordinates of the virtual center point of the images.

The experimental results of the computation time used by the proposed algorithm are shown in Table. 4. As can be seen, the proposed method shows high efficiency. Fig. 12 and Fig. 13, respectively, show the image match pairs of the asteroids Bennu and Ryugu. The right half of the figure shows the local detail of an image pair. We use ISIS's *qview* to display asteroid images. The first image on the left half of the figure is the reference image, and the other images are the images with overlapping relationships. The red dot in the figure is a homologous point for the image pairs, which facilitates showing the local details of the overlapping images. It demonstrates that the proposed algorithm can derive the correct image match relationship.

Table 4 Test data for asteroid remote sensing images containing invalid pixels

	Bennu（2018）			Ryugu
Number of images	133	417	942	391
Time spent on KD tree/s	<1	<1	1-2	<1
Time spent on ISIS	—	—	—	—

Note: “—” means unable to process.

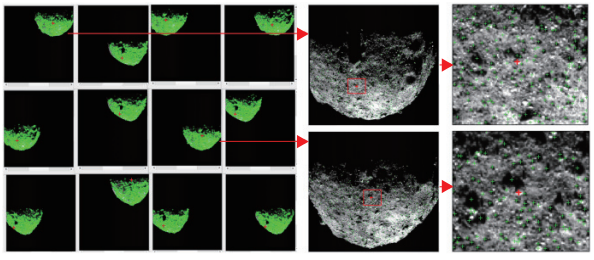

Fig. 12 Image matching pairs for preliminary survey phase of Bennu

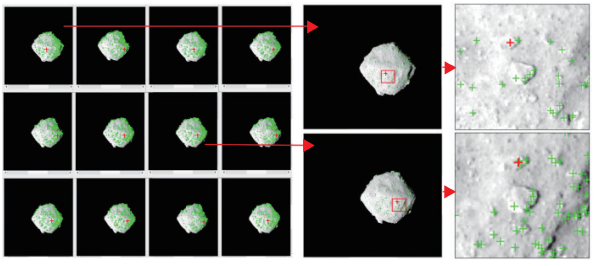

Fig. 13 Image matching pairs for characterization phase of Ryugu

2.4 Photogrammetric Processing Results

2.4.1 Construction of control network

A high-quality control network is crucial for bundle adjustment. Here, we use NASA ASP’s software tools, namely *ipfind* and *ipmatch*, to obtain the tie points. Specifically, *ipfind* is first used to detect feature points, and then *ipmatch* is used to match conjugate points. Then, the image matching files generated by *ipmatch* are converted into a PVL (Parameter Value Language) format control network file, which can be directly used by the ISIS’s bundle adjustment software tool *jigsaw*.

We conducted experiments on the four datasets, and the specific bundle adjustment result is shown in Table. 5.

Table 5 Bundle adjustment results of test data

Test data	Total images in control network	Total match pairs	Total control points	Total control measures	Sigma 0
Test 1	5 453	48 940	445 565	1 506 597	0.17
Test 2	2 553	34 143	122 002	459 977	0.18
Test 3	942	15 527	251 067	920 735	0.15
Test 4	391	4 086	52 989	199 027	0.27

2.4.2 Bundle Adjustment

The effectiveness of bundle adjustment largely depends on the accuracy of the determination of the image overlapping relationship. If there is a mismatched image pair, it will lead to incorrect tie points, thereby affecting the refinement of the position and attitude of the spacecraft and reducing the accuracy of the bundle adjustment results. Indeed, the quality of the bundle adjustment results also provides a basis for verifying the correctness of the image match pairs. If the adjustment results show high accuracy, it indicates that the proposed method is effective in obtaining image match pairs.

This study uses the *jigsaw* application provided by USGS ISIS for bundle adjustment. It is generally considered that when the residual value of the image observation (i.e., tie point) is less than 1 pixel and the adjustment result’s index, namely the Sigma0 value, is less than 0.5, a satisfactory adjustment result can be considered obtained.

As can be seen from Table. 5, the Sigma0 values of the four datasets are all less than 0.3, indicating that satisfactory bundle adjustment results are obtained for all cases. TheRoot-Mean-Square Error (RMSE) of the image observation for each image after bundle adjustment is shown in Fig. 14 to Fig. 17. For Test 1, most of the residual values of Bennu images in the detailed survey stage are within 0.2 pixels, and a small part are within 0.4 pixel. For Test 2 the Vesta images in the HAMO stage most of the image residual values are within half a pixel, and a small part are between half a pixel and one pixel. In the case of Test 3, namely the Bennu images in the preliminary survey stage, most of the image residual values of the bundle adjustment are within 0.3 pixels, and a small part are within half a pixel. Since Test 4 contains Ryugu images with different resolutions, the image residual values are larger, but basically within one pixel. The small image residual values of bundle adjustment indirectly indicate the correctness of the image match pairs.

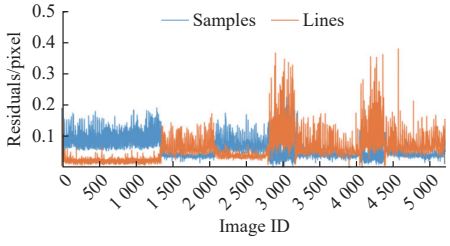

Fig. 14 RMSE values of control measure residuals for each image of Test 1 data

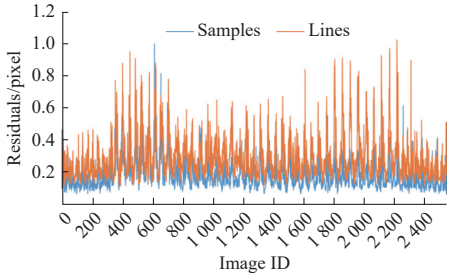

Fig. 15　Same as Fig. 14 but for Test 2 data

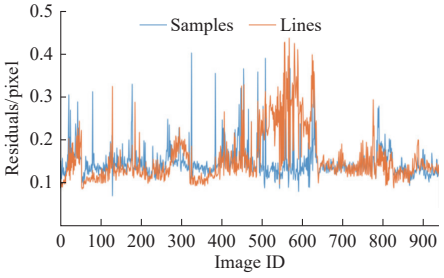

Fig. 16　Same as Fig. 14 but for Test 3 data

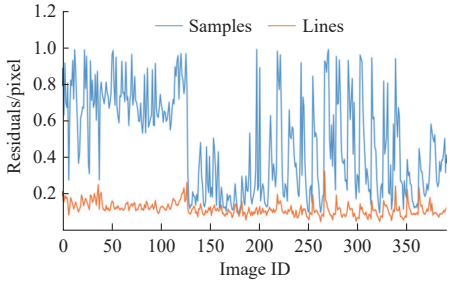

Fig. 17　Same as Fig. 14 but for Test 4 data

The geometric positioning accuracy of tie points is shown in Fig. 18 to Fig. 21. The geometric positioning accuracy of the tie points refers to the position estimation accuracy of the tie points in three-dimensional space, which is derived based on the posterior variance estimation in the bundle adjustment process. It reflects the intrinsic consistency of geometric accuracy between stereo images and belongs to the category of relative positioning accuracy.

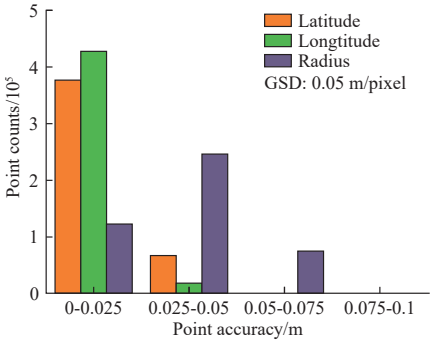

Fig. 18　Geometric positioning accuracy of control points for Test 1 data

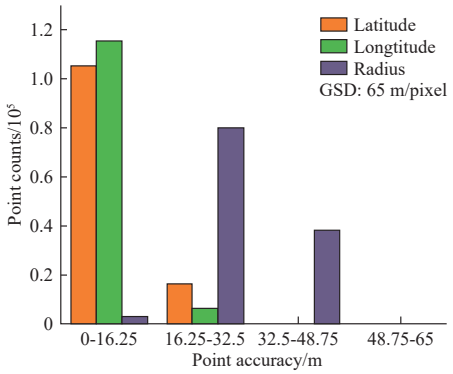

Fig. 19　Same as Fig. 18 but for Test 2 data

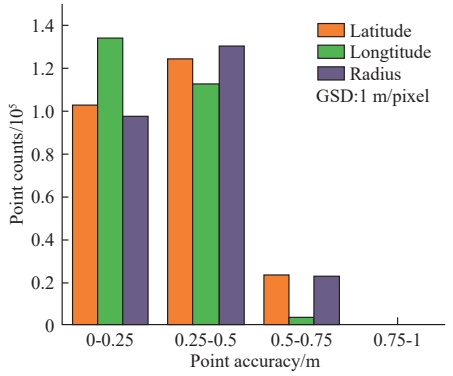

Fig. 20　Same as Fig. 18 but for Test 3 data (We use 1 m as the average resolution)

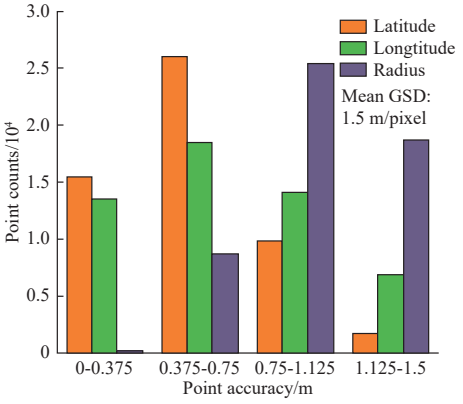

Fig. 21　Same as Fig. 18 but for Test 4 data (We use 1.5 m as the average resolution)

Considering the image resolutions of test data, the Bennu images in the detailed survey stage (i.e., Test 1) can achieve an average positioning accuracy of better than 0.25 pixels in the plane direction and about 0.5 pixels in the elevation direction; the Vesta images in Test 2 can achieve a positioning accuracy of about better than 0.3 pixels in the plane direction and about 0.8 pixels in the elevation direction; the Bennu images in the preliminary survey stage (i.e., Test 3) can achieve an average positioning accuracy of about 0.5 pixel for both plane and elevation

directions; and the Ryugu images in Test 4 can achieve an average positioning accuracy of about 1 pixel for both plane and elevation directions. For Tests 3 and 4, we use 1 and 1.5 m as the average resolutions, respectively. Such geometric positioning accuracy is basically the same as the geometric positioning accuracy of remote sensing images of Earth observation satellites.

2.4.3 Orthophoto mosaic

The accuracy of the orthophoto mosaic can truly reflect the geometric positioning accuracy of adjacent images. This can also demonstrate the effectiveness of the determination of the image match pairs. If the overlapping images are not calculated correctly, the geometric errors between overlapping images cannot be removed by bundle adjustment. Then, it may lead to the geometric misalignment of overlapping orthophotos. After bundle adjustment, we used *cam2map* provided by USGS ISIS for orthorectification. We use the orthophoto mosaic of asteroid Vesta with longitudes ranging from 0 to 360° and latitudes ranging from –60° to 50° generated using Test 2 data is shown in part a of Fig. 22. Note that the remote sensing images returned by the DAWN asteroid exploration mission lack effective image coverage in the North Pole. It can be seen that the discrepancies in adjacent DOMs are less than one pixel in part b of Fig. 22. In particular, the effect of the DOM mosaic can be visualized in the adjacent image areas with steeper terrain within the red frame in the figure. This indicated that the generated DOMs showed high relative accuracy. It also demonstrated that the bundle adjustment delivered a good result, and the discrepancies between the adjacent images were removed. The updated external orientation parameters derived from the bundle adjustment provided consistent geometric accuracy for adjacent images.

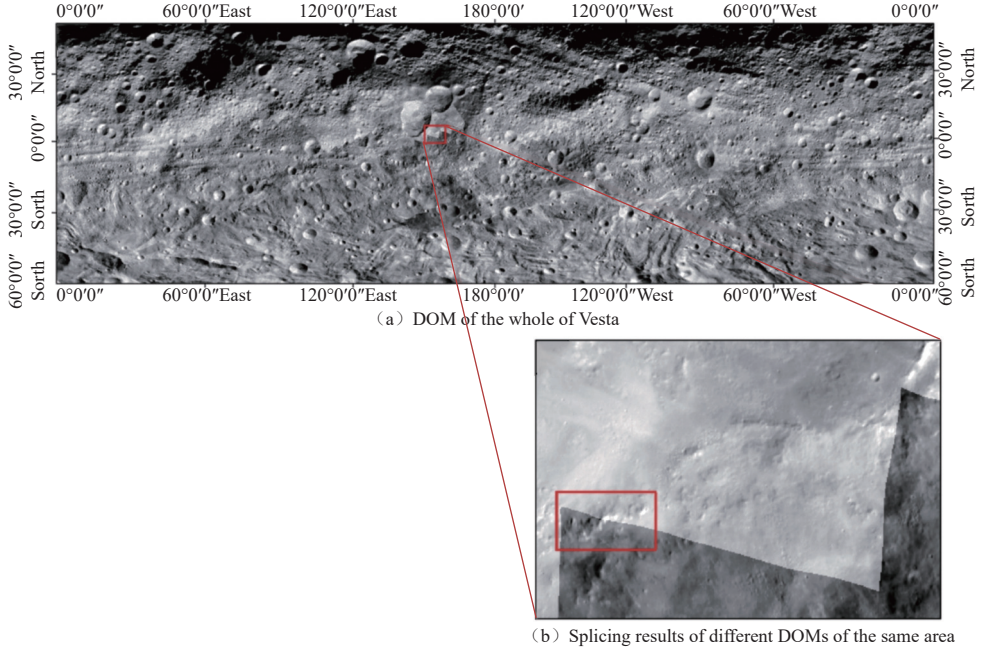

（a）DOM of the whole of Vesta

（b）Splicing results of different DOMs of the same area

Fig. 22 Fig.22 DOM mosaic effect of Vesta

2.4.4 SPC reconstruction

We selected some of the images in Test 2 after bundle adjustment for the 3D reconstruction experiment. The specific procedure for SPC reconstructing using the KD tree method is as follows:

1) Select an area as a candidate area for the experimental region, input the latitude and longitude range of the target area, and screen all the images of the candidate area to form an initial or pre-selected image collection;

2) Calculate the overlapping relationship among the pre-selected images based on the spatial search method of KD tree. According to the image matching pairs obtained from the KD tree and the target area, the images in the experimental region are preliminarily selected to form the experimental region image collection (as shown in Fig. 23(b));

3) Combined with the SPC reconstruction requirements, the five images that best meet the SPC reconstruction requirements are quickly screened out from the experimental area image collection based on the information of the image's incidence angle, observation angle, spacecraft's azimuth and solar azimuth ((as shown in Fig. 23(c)) to generate the DEM. The area for the SPC experiment in this study was 500 × 500 pixels.

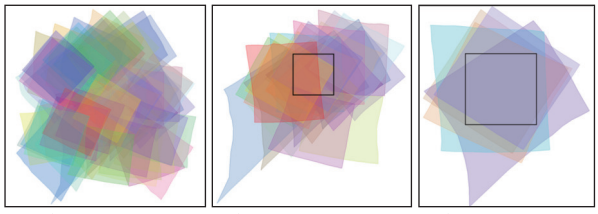

（a）Original images for the large test area (70 images)　（b）Preliminary selected overlapping images using proposed KD tree-based method (22 images)　（c）Selected optimal images that meet illumination and observation requirements of SPC (5 images)

Note: The black box in the figure is the experimental area for SPC reconstruction.

Fig. 23　The process of selecting optimal images for SPC reconstruction

Fig. 24 shows the observation and illumination conditions of the selected Vesta images. Fig. 24(a) shows the distribution of the solar ground azimuth and incidence angle, and Fig. 24(b) shows the distribution of the spacecraft ground azimuth and emission angle. These two figures are plotted in polar coordinates because this can intuitively represent the observation and illumination conditions. The polar angle in Fig. 24 corresponds to the solar ground azimuth, and the polar radius corresponds to the solar incidence angle (0° indicates close to the center). As can be seen from the figure, the incidence angles of the first four selected images are different, which can provide complementarity for the terrain. The polar angle and polar radius in part b of Fig. 24 correspond to the azimuth and emission angle of the spacecraft, respectively. As can be seen from the figure, the spacecraft's azimuth angles of the five selected images are roughly distributed in all directions, which can improve the terrain reconstruction quality and supplement the shadow areas.

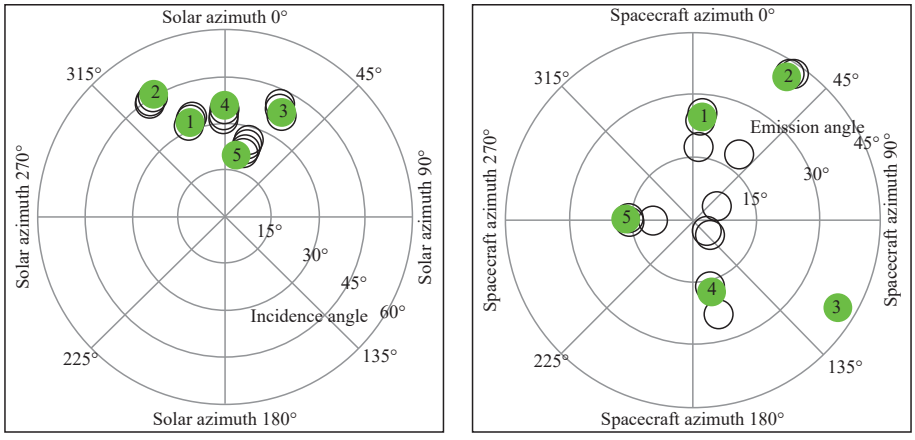

（a）Solar azimuth and incidence angle　（b）Space-craft azimuth and emission angle

Note: The green circles in the figure represent the five images that are finally selected and basically meet the requirements of SPC.

Fig. 24　Illumination and observation and conditions of Vesta images for SPC reconstruction

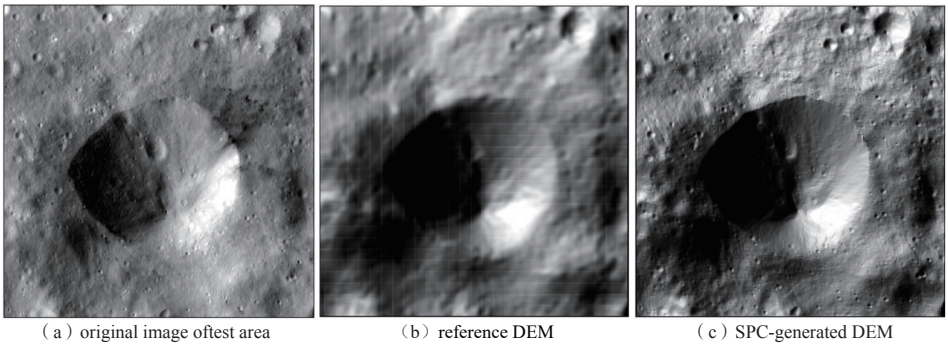

（a）original image oftest area　（b）reference DEM　（c）SPC-generated DEM

Fig. 25　SPC reconstruction results (with a resolution of 100 m/pixel)

Using the five selected images, we generated a DEM with a size of 500 × 500 pixels by SPC (as shown in Fig. 25). The DEM has a grid spacing of 100 m. From the results, it can be seen that the DEM generated by SPC has a spatial resolution that is essentially the same as the original image, which indicates that the proposed method can provide good support for optimal image selection for SPC reconstruction.

In order to analyze the absolute elevation accuracy of the DEM generated by SPC, we compared the DEM generated by SPC with the officially provided DEM (referred to as the reference DEM). Specifically, we calculated the elevation values of sample points in the DEM generated by SPC and the reference DEM, and then we calculated the differences between them. The results are shown in Fig. 26 and Fig. 27. It can be seen from Fig. 26 that the DEM generated by SPC is consistent with the reference DEM. The RMSE values of the height difference is 61.16 meters, and the average error is 49.71 meters. Both are less than one pixel (65 m/pixel). As can be seen from the pixel-by-pixel height difference map in Fig. 27, the elevation differences are basically within 1 pixel, and may reach 2 or 3 pixels in the pits.

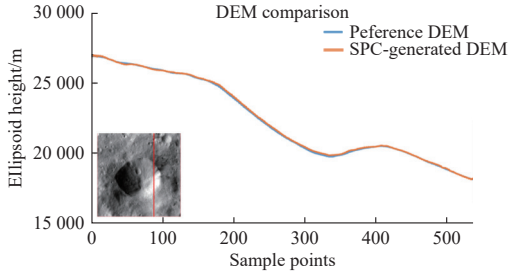

Note: Red line in the lower left corner indicates the location of sample points.

Fig. 26 Comparison results of SPC-generated DEMs with reference DEM

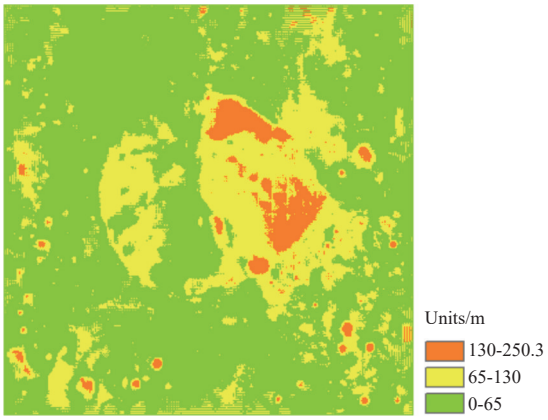

Fig. 27 Pixel-by-pixel height difference map between SPC-generated DEM and the reference DEM

3 Conclusions

In photogrammetric processing, accurately and efficiently determining image match pairs among large numbers of images is fundamental and crucial for creating high-precision planetary remote sensing mapping products. Existing methods like USGS ISIS in planetary mapping have issues. For instance, when determining the overlapping relationship of thousands of asteroid images, USGS ISIS is time-consuming and may even fail to generate a valid overlapping relationship file, preventing subsequent control network construction and bundle adjustment. Also, existing methods can't handle low-resolution images with invalid pixels from the approach stage as footprint coordinates can't be derived. Thus, they can't meet the demands of processing large-scale, unordered asteroid remote sensing images.

This paper presents an efficient image match pair determination method based on KD-tree fast search. It suits massive asteroid remote sensing images, offering high efficiency and accuracy. For images with invalid pixels where ISIS can't calculate footprint coordinates or overlapping relationships, this method can still determine match pairs. Moreover, based on the determined match pairs, it can effectively help select optimal images for SPC reconstruction. So, for asteroid remote sensing images, this method has high practical value in the photogrammetric processing projects.

References

[1] WEI T. Orbit determination of the asteroid (469219) Kamoòalewa and its error analysis[J]. Chinese Astronomy and Astrophysics, 2021, 45: 402-411.

[2] MARCH R E. OSIRIS-REx: a NASA asteroid space mission[J/OL]. International Journal of Mass Spectrometry, 2021, 469: 116677. https://www.sciencedirect.com/science/article/abs/pii/S1387380621001573.

[3] YADA T, ABE M, OKADA T, et al. Preliminary analysis of the Hayabusa2 samples returned from C-type asteroid Ryugu[J]. Nature Astronomy, 2022, 6: 214-220.

[4] SEABROOK J A, DALY M G, BARNOUIN O S, et al. Building a high-resolution digital terrain model of Bennu from laser altimetry data[J/OL]. The Planetary Science Journal, 2022, 3: 265. https://iopscience.iop.org/article/10.3847/PSJ/aca011.

[5] BENNETT C A, DELLAGIUSTINA D N, BECKER K J, et al. A high-resolution global basemap of (101955) Bennu[J/OL]. Icarus, 2021, 357: 113690. https://www.sciencedirect.com/science/article/abs/pii/S0019103520300816.

[6] KIM J，LIN S Y ，XIAO H F. Remote sensing and data analyses on planetary topography[J/OL]. Remote Sensing，2023，25：2954. https://www.mdpi.com/2072-4292/15/12/2954.

[7] LAURETTA D S，BALRAM-KNUTSON S S，BESHORE E，et al. OSIRIS-Rex：sample return from asteroid（101955）Bennu[J]. Space Science Reviews，2017，212：925-984.

[8] RUSSELL C T，RAYMOND C A. The dawn mission to Vesta and Ceres[J]. Space Science Reviews，2011，163：3-23.

[9] BARNOUIN O S，DALY M G，PALMER E E，et al. Digital terrain mapping by the OSIRIS-Rex mission[J/OL]. Planetary and Space Science，2020，180：104764. https://www.sciencedirect.com/ science/ article/abs/pii/S0032063318303805

[10] PREUSKER F，SCHOLTEN F，ELGNER S，et al. The MASCOT landing area on asteroid（162173）Ryugu：stereo-photogrammetric analysis using images of the ONC onboard the Hayabusa2 spacecraft. Astron[J/OL]. Astronomy & Astrophysics，2019，632：L4. https:// www.researchgate.net/publication/337227043_The_MASCOT_landing_ area_on_Asteroid_162173_Ryugu_Stereo-photogrammetric_ analysis_ using_images_of_the_ONC_cameras_onboard_the_Hayabusa2_spacec raft.

[11] ROATSCH TH，KERSTEN E，MATZ K D，et al. High-resolution Vesta high altitude mapping orbit（HAMO）atlas derived from dawn framing camera images[J]. Planetary and Space Science，2012，73：283-286.

[12] ROATSCH TH，KERSTEN E，MATZ K D，et al. High-resolution Vesta low altitude mapping orbit atlas derived from dawn framing camera images[J]. Planetary and Space Science，2013，85：293-298.

[13] DELLAGIUSTINA D N，BENNETT C A，BECKER K，et al. Overcoming the challenges associated with image-based mapping of small bodies in preparation for the OSIRIS-Rex mission to（101955）Bennu[J]. Earth and Space Science，2018，5：929-949.

[14] EDMUNDSON K L，BECKER K J，BECKER T L，et al. Photogrammetric processing of Osiris-Rex images of asteroid（101955）Bennu[C]//Proceedings of ISPRS Annals of the Photogrammetry，Remote Sensing and Spatial Information Sciences. [S. l.]: ISPRS，2020：587-594.

[15] SCHOLTEN F，PREUSKER F，ELGNER S，et al. The Hayabusa2 lander MASCOT on the surface of asteroid（162173）Ryugu：Stereo-photogrammetric analysis of MAS-Cam image data[J/OL]. Astronomy & Astrophysics. 2019，632：L5. https://www.aanda.org/articles/ aa/full_html/2019/12/aa36760-19/aa36760-19.html.

[16] KIRK R L，ARCHINAL B A，GADDIS L R，et al. Lunar cartography：progress in the 2000s and prospects for the 2010s[C]//Proceedings of The International Archives of the Photogrammetry，Remote Sensing and Spatial Information Sciences，2012，39(B4)：489-494.

[17] ROBBINS S J，KIRCHOFF M R，HOOVER R H. Fully controlled 6 meters per pixel mosaic of Mars's south polar region[J/OL]. Earth and Space Science，2020，7：e2019EA001054. https://doaj.org/article/ 40cbc0d1e6f24f60900e3f75ab86ee3b#:~:text=The%20Context%20Camera%20%28CTX%29%2C%20aboard%20MRO%2C%20has%20returned,Mars%20at%20%E2%89%885%E2%80%936%20m%2Fpx%2C%20providing%20nearly%20global%20coverage.

[18] GENG X，XU Q，WANG J，et al. Generation of large-scale orthophoto mosaics using MEX HRSC images for the candidate landing regions of China's first Mars mission[J]. IEEE Transactions on Geoscience and Remote Sensing，2022，60：1-20.

[19] ROBBINS S J，KIRCHOFF M R，HOOVER R H. Fully controlled 6 meters per pixel equatorial mosaic of Mars from Mars reconnaissance orbiter context camera images，Version 1[J/OL]. Earth and Space Science，2023，10：e2022EA002443. https://agupubs.onlinelibrary.wiley.com/doi/full/10.1029/2022EA002443.

[20] LIANG Y B，LI D Q，FENG C Y，et al. Efficient match pair selection for matching large-scale oblique UAV images using spatial priors[J]. International Journal of Remote Sensing，2021，42(23)：8878-8905.

[21] JIANG S，JIANG W S. Efficient match pair selection for oblique UAV images based on adaptive vocabulary tree[J]. ISPRS Journal of Photogrammetry and Remote Sensing，2020，161：61-75.

[22] JIANG S，MA Y C，LIU J H，et al. Efficient match pair retrieval for large-scale UAV images via graph indexed global descriptor[J]. IEEE Journal of Selected Topics in Applied Earth Observations and Remote Sensing，2023，16：9874-9887.

[23] RUPNIK E，NEX F，REMON DINO F. Automatic orientation of large blocks of oblique images[J]. The International Archives of the Photogrammetry，Remote Sensing and Spatial Information Sciences，2013，XL-1-W1：299-304.

[24] CHEN X Y L，LÄBE T，MILIOTO，et al. OverlapNet：Loop closing for LiDAR-based SLAM[C]//Proceedings of the 2020 Robotics: Science and Systems Conference (RSS 2020). Corvallis, Oregon, USA: [s. n.]: 2020.

[25] CHEN X Y L，LÄBE T，MILIOTOet al. OverlapNet：A siamese network for computing LiDAR scan similarity with applications to loop closing and localization[J]. Autonomous Robots, 2022，46: 61-81.

[26] EDMUNDSON K L，COOK D A，THOMAS O H，et al. Jigsaw：the ISIS3 bundle adjustment for extraterrestrial photogrammetry[J]. ISPRS Annals of the Photogrammetry，Remote Sensing and Spatial Information Sciences，2012，1：203-208.

[27] BEYER R A，ALEXANDROV O，MCMICHAEL S. The Ames stereo pipeline：NASA's open-source software for deriving and processing terrain data[J]. Earth and Space Science，2018，5：537-548.

[28] SHEAN D E，ALEXANDROV O，MORATTO Z M，et al. An Automated，Open-source pipeline for mass production of digital elevation models（DEMs）from very-high-resolution commercial stereo satellite imagery[J]. ISPRS Journal of Photogrammetry and Remote Sensing，2016，116：101-117.

[29] PALMER E E，GASKELL R，DALY M G，et al. Practical Stereophotoclinometry for modeling shape and topography on planetary missions[J/OL]. The Planetary Science Journal，2022，3：102. https://iopscience.iop.org/article/10.3847/PSJ/ac460f.

[30] LIU P Y，GENG X，LI T，et al. The generation of high-resolution mapping products for the lunar south pole using photogrammetry and photoclinometry[J/OL]. Remote Sensing，2024，16，2097. https://www.mdpi.com/2072-4292/16/12/2097.

[31] SILPA-ANAN C，HARTLEY R. Optimised KD trees for fast image descriptor matching[C]//Proceedings of 2008 IEEE Conference on Computer Vision and Pattern Recognition（CVPR）. [S. l.]: IEEE, 2010.

[32] MUJA M，LOWE D G. Scalable nearest neighbor algorithms for high dimensional data[J]. IEEE Transactions on Pattern Analysis and Machine Intelligence，2014，36：2227-2240.

[33] CHEN X. GÜTTEL S. Fast and exact fixed-radius neighbor search based on sorting[J/OL]. Computer Science，2024，10：1929.

https://arxiv.org/abs/2212.07679.

[34] TIWARI V. Developments in KD tree and KNN searches[J]. International Journal of Computer Applications，2023，185：17-23.

[35] BEHLEY J，STEINHAGE V，CREMERS A. B. Efficient radius neighbor search in three-dimensional point clouds[C]//Proceedings of 2015 IEEE International Conference on Robotics and Automation（ICRA）. [S. l.]: IEEE, 2015: 3625-3630.

[36] AL ASAD M M，PHILPOTT L C，JOHNSON C L，et al. Validation of Stereophotoclinometric shape models of asteroid（101955）Bennu during the OSIRIS-Rex mission[J/OL]. The Planetary Science Journal，2021，2(2)：82. https://iopscience.iop.org/article/10.3847/PSJ/abe4dc.

[37] GASKELL R W，BARNOUIN O S，DALY M G，et al. Stereophotoclinometry on the OSIRIS-Rex mission：mathematics and methods[J/OL]. The Planetary Science Journal，2023，4(4)：63. https://iopscience.iop.org/article/10.3847/PSJ/acc4b9.

[38] ADAM C D，MCCARTHY L K，LEONARD J M，et al. Stereophotoclinometry for OSIRIS-Rex spacecraft navigation[J/OL]. The Planetary Science Journal，2023，4：167. https://iopscience.iop.org/article/10.3847/PSJ/ace31d.

[39] WEIRICH J，PALMER E. E，DALY M G，et al. Quality assessment of Stereophotoclinometry as a shape modeling method using a synthetic asteroid[J/OL]. The Planetary Science Journal，2022，3：103. https://iopscience.iop.org/article/10.3847/PSJ/ac46d2.

[40] LIU W C，WU B. Influence of solar incidence angle on single-image photoclinometry for precision lunar topographic mapping[J]. ISPRS Journal of Photogrammetry and Remote Sensing，2021，182：208-227.

[41] BROWN R A. Building a balanced KD tree in o（kn log n）time[J]. Computer Science，2015，4(2)：50-68.

The Author Profiles

ZHANG Jiujiang(2000−), Male, Master's degree student, Main Research Direction: asteroid photogrammetric processing and three-dimensional modeling.

Address: Zhengzhou Campus, Henan University, No. 379, North Section of Mingli Road, Zhengdong New District, Zhengzhou City, Henan Province, 450046，China.

E-mail: zhangjiujiang@henu.edu.cn

GENG Xun(1982−), Male, Associate Professor, Doctoral Supervisor, Main Research Direction: Aerospace photogrammetry, planetary remote sensing mapping, real-time three-dimensional reconstruction. Corresponding author of this article.

Address: Zhengzhou Campus, Henan University, No. 379, North Section of Mingli Road, Zhengdong New District, Zhengzhou City, Henan Province, 450046，China.

E-mail: gengxun@henu.edu.cn

一种海量无序小行星遥感影像匹配对快速确定方法

张九江[1,2,3]，耿　迅[1,2,3]，于君明[4]，刘　杰[4]，刘朋英[1,2,3]，彭　真[1,2,3]，马　鑫[3,5]

（1. 河南大学 地理科学与工程学部地理科学学院，郑州 450046；
2. 地理信息工程国家重点实验室，西安 710054；
3. 河南省时空大数据产业技术研究院，郑州 450046；
4. 中国电子科技集团公司第二十七研究所，郑州 450047；
5. 河南大学 计算机与信息工程学院，开封 475004）

摘　要：针对海量无序小行星影像，提出了一种基于KD树空间索引快速搜索的高效影像重叠关系分析方法。以贝努、灶神星、龙宫等小行星探测任务的影像数据为实验对象，将提出的影像匹配对算法与美国地质调查局ISIS的相应模块进行系统比较，以评估其在效率和精度方面的性能。结果表明，在处理超过一千幅影像时，所提出的方法在保证影像重叠关系的正确性和光束法平差精度的前提下，极大地提升了获取影像匹配对的效率。同时，根据获得的影像匹配对，可以快速优选出符合立体光度法要求的影像，有效提高了小行星影像三维重建模型的质量。

关键词：小行星探测；摄影测量；影像匹配；KD树；影像匹配对

[责任编辑：宋宏，英文审校：宋利辉]